J Intell Robot Syst (2017) 88:635–654
DOI 10.1007/s10846-016-0464-7

Aerial Images-Based Forest Fire Detection for Firefighting Using Optical Remote Sensing Techniques and Unmanned Aerial Vehicles

Chi Yuan · Zhixiang Liu · Youmin Zhang

Received: 5 October 2016 / Accepted: 20 December 2016 / Published online: 5 January 2017

Abstract Due to their fast response capability, low cost and without danger to personnel safety since there is no human pilot on-board, unmanned aerial vehicles (UAVs) with vision-based systems have great potential for monitoring and detecting forest fires. This paper proposes a novel forest fire detection method using both color and motion features for processing images captured from the camera mounted on a UAV which is moving during the whole mission period. First, a color-based fire detection algorithm with light computational demand is designed to extract fire-colored pixels as fire candidate regions by making use of chromatic feature of fire and obtaining fire candidate regions for further analysis. As the pose variations and low-frequency vibrations of UAV cause all objects and background in the images are moving, it is challenging to identify fires defending on a single motion based method. Two types of optical flow algorithms, a classical optical flow algorithm and an optimal mass transport optical flow algorithm, are then combined to compute motion vectors of the fire candidate regions. Fires are thereby expected to be distinguished from other fire analogues based on their motion features. Several groups of experiments are conducted to validate that the proposed method can effectively extract and track fire pixels in aerial video sequences. The good performance is anticipated to significantly improve the accuracy of forest fire detection and reduce false alarm rates without increasing much computation efforts.

Keywords Unmanned aerial vehicles · Forest fires · Optical flow · Optical remote sensing · Fire detection · Image processing

C. Yuan · Z. Liu · Y. Zhang (✉)
Department of Mechanical and Industrial Engineering, Concordia University, 1455 de Maisonneuve Blvd. W., Montreal, QC H3G 1M8, Canada
e-mail: youmin.zhang@concordia.ca

C. Yuan
e-mail: chiyuan996@gmail.com

Z. Liu
e-mail: lzhx180@gmail.com

Y. Zhang
Shaanxi Key Laboratory of Complex System Control and Intelligent Information Processing, Xi'an University of Technology, Xi'an, Shaanxi 710048, China

1 Introduction

Forests play numerous critical characters in nature. They stabilize and fertilize soil, purify water and air, store carbon, moderate climate, and nurture environments abundant in biodiversity. From an economic perspective, forests also contribute a vast number of jobs opportunities and billions of dollars to a country's economic wealth [1]. Unfortunately, forest fires have become a serious natural danger [2]. Every year, millions of hectares of forest and human infrastructures are destroyed by forest fires, lives are threatened,

injured or even killed, thousands of people have to leave their home, and a great deal of personnels, facilities and money are used to extinguish these fires [1, 3]. Forest fires fighting is thereby seen as one of the most significant roles in the preservation of natural resources and protection of personal and property security [2, 4]. In particular, due to the fast convection propagation and long combustion period of forest fires, early detection of forest fires is considered to be a predominant way for minimizing the destruction that is probably caused by fires [5].

Massive efforts have been devoted to the detection of forest fires before they develop into uncontrollable. Traditional forest fire monitoring and detection methods employing watchtowers and human observers to monitor the surroundings usually require extensive labour forces, are subject to the spatio-temporal limitations, and potentially threaten personnel safety. Along with the new development of technologies, in the past decades, monitoring of forests and detection of forest fires primarily rely on ground fire monitoring systems, manned aircraft, and satellites. However, different technological and practical problems exist in each of these systems. Ground monitoring system is normally fixed in a specific place and may suffer from limited surveillance ranges. Manned aircraft is usually large and expensive; meanwhile, the hazardous environments, harsh weather, and operator fatigue can potentially threaten the life of the pilot. Satellite systems are typically expensive for launching and less flexible for deployment and technology updates; moreover, their spatio-temporal resolutions sometimes may be difficult to meet the requirement of detailed data capture and operational forest fire detection [1].

As a promising substitution of traditional and current forest fire detection approaches, the integration of unmanned aerial vehicles (UAVs) with remote sensing techniques serving as a powerful tool for operational forest fire detection applications has attracted worldwide increasing attention [1, 6, 7]. Alternatively, UAVs with computer vision based remote sensing systems onboard have been an increasingly realistic choice by providing low-cost, safe, rapid, and mobile characteristics for forest fire monitoring and detection. They are capable of meeting the crucial spatio-temporal and spectral resolution requirements [7]. They can also enable the execution of long-term, dull, and repetitive missions beyond human capabilities. In addition, vision-based detection technique can capture and deliver intuitive and highly real-time information as well as cover a wide viewing range conveniently with reduced development cost. Accordingly, a great number of research activities, in recent years, have been carried out for UAVs-based forest fire monitoring and detection applications [3, 8, 10–20].

In the existing research works, vision-based systems generally detect fires according to three features: color, motion, and geometry [21]. Especially, most of researchers tend to combine the color and motion features to provide more reliable fire detection results, rather than using single feature. In [22], the RGB (Red, Green and Blue)/HSI (Hue, Saturation, Intensity) color models are adopted, the disordered characteristics of flames are dynamically analysed to verify the possibility of fire occurrence. The authors of [23] consider the combination of motion and color features along with analysing fire flicker in wavelet domain to detect forest fires in videos. A real-time fire detection method using an adaptive background subtraction algorithm is designed in [24] in order to extract foreground information; a statistical fire color model is then adopted to check the existence of fires. In their successive work [25], a rule-based generic color model is used for the classification of fire pixels, experimental results have demonstrated the significantly improved fire detection performance of utilizing this model. Gunay [26] proposes a four sub-algorithms based approach and a data fusion method for video-based wildfires detection at night and combining decisions from sub-algorithms, respectively. Later on, a continuation of this work is to develop an entropy-functional-based online adaptive decision fusion (EADF) framework for fires detection applications, both video-based and experimental results have verified the effectiveness of the proposed algorithm [27]. In [28], a color-lookup table is designed with massive training images for identifying the existence of possible fire regions and a temporal variation is also adopted to distinguish fires from fire color analogous objects. A support vector machine (SVM) based fire detection method, which employs a luminance map to remove non-fire pixels regions, is introduced in [29]. Furthermore, a two-class SVM classifier with a radial basis function kernel is designed for the verification of fire pixels in [29]; but it is difficult to apply

this classifier in real-time due to its excessive requirement for computation time. [8, 9] address approaches intended to effectively extract fire-pixels by employing the advantages of Lab color model capable of revealing fires' color feature obviously, while Otsu segmentation method is used in [8] as well; experimental results validate that the proposed method can effectively extract forest fire pixels.

Although a variety of forest fire detection methodologies have been developed, only several research studies have considered forest fire scenarios and few relative experiments have been conducted for monitoring and detecting forest fires using UAVs [3, 11, 14–20]. Several challenging issues existing in the practice contribute to these phenomena, such as choosing the suitable UAV platforms, remote sensing payloads and sensors, algorithms for autonomous guidance, navigation and control (GNC), as well as using UAVs in combination with other remote sensing techniques [1]. Among these challenges, the combination of UAV and remote sensing techniques is particularly more challenging. In general, the developed vision-based fire detection methods are applied with stationary cameras by separating fires from the static backgrounds. However, the techniques using/involving motion features of fire for fire detection may fail to perform as expected when cameras are attached to UAVs which are moving during the entire operation period. Under this circumstance, objects (including the interested objects and background) in the captured images are all moving, which is the primary cause of the failure in fire detection [30]. In order to solve this problem, several techniques are adopted by researchers. In [31], a background subtraction approach is developed with combination of intensity threshold, motion compensation, and pattern classification. Huang [32] presents an accumulative frame differencing method for detecting the moving pixels and combining the homogeneous regions of these pixels in the frame after image segmentation. As one of the predominant promising motion analysis techniques, optical flow is widely employed in other studies [33, 34]. Despite this, the motion of camera is assumed to be *priori* known in these methods. More effective online motion estimation strategies are strongly demanded.

In order to solve the problems mentioned above, this research studies a new vision-based forest fire detection method using UAVs. Both color and motion features are utilized for improving the robustness of fire detection, which constitute a two-layered system architecture. The first layer is the color-based fire detection which is designed to segment the fire candidate regions using a light computation algorithm, while the second layer is the motion-based fire detection which is designed to further analyse the segmented fire candidate regions. This design philosophy is intended to significantly reduce the computation time without sacrificing the accuracy of fire detection. The general design procedure of this study can be illustrated as follows: 1) regarding the color-based detection method, chromatic features in the so-called Lab color space is applied for detecting fire-colored pixels and eliminating non-fire colored pixels; 2) for the motion-based detection approach, two types of optical flow approaches are adopted to further analyse the segmented fire-colored regions from color-based detection, one is a classic artificial optical flow [35] for estimating the motion (both direction and velocity) of camera; the other optical flow is a newly developed technique by [34] for fire detection, this optical flow is based on the subtraction of the motion information of camera obtained from the first optical flow; 3) finally, the fire pixel candidates can be further determined according to a relatively empirical discrimination rule. Once the fire pixel candidates are confirmed, the binary feature images can be produced after thresholding and performing morphological closing on the motion vectors. A Blob Counter scheme is then used to track the fire regions in each binary feature image. Experiments on videos of forest fires and indoor tests with charge-coupled device (CCD) camera onboard UAV are both carried out for the verification of the effectiveness of the proposed forest fire detection method.

The rest of this paper is organized as follows. Section 2 provides some preliminary descriptions of the UAV-based forest fire detection system, color-based forest fire detection method, and motion-based forest fire detection approach. Section 3 describes the proposed forest fire detection algorithm in twofold steps: 1) fire-colored pixels detection using chromatic features in Lab color space, and 2) moving regions extraction and fire detection using two types of optical flow methods. Section 4 introduces the control strategies that are developed to deploy the UAV for

fire search and detection. Section 5 addresses the scenarios description and results analyses of the conducted experiments. Finally, concluding remarks and future works are drawn in the last section.

2 Preliminaries

2.1 General Description of UAV-Based Automatic Forest Fire Detection System

As illustrated in Fig. 1, a typical UAV-based forest fire detection system consists of a single UAV or a team of UAVs (with different kinds of sensors onboard) for forest fire search, a dedicated central ground station for mission planning and data display, communication system for data transmission and command distribution, and visual/infrared cameras for capturing images for forest fires detection.

The UAVs-based forest fire detection mission can be conducted as follows: 1) first, a fleet of UAVs fly along respective trajectories formulated in advance, meanwhile the onboard cameras capture images on the ground and vision-based fire detection system searches for any suspicious fires in the obtained images; 2) once the fire is detected and preliminarily confirmed by the fire detection system onboard (when the onboard device's computation capabilities are powerful enough) or on the ground (when the onboard device's computation capabilities are insufficient), a fire alarm is then alerted and suspicious fire images are to be captured by the cameras mounted on UAVs; 3) these images are then sent to both mobile devices and the ground station for firefighters or relevant staffs to check and make further decisions on the probabilities of occurrence of forest fires.

2.2 Fire-Colored Regions Detection

Color-based object detection, which is one of the earliest detection techniques used in vision-based forest fire detection applications, is by far popularly adopted [36]. Generally, fire flames display reddish colors, which range from red to yellow during the burning process [22]. Therefore, the range of fire color can be treated as an interval of color values between red and yellow. Based on this phenomenon, the majority of the existing color-based fire detection methods make use of RGB color model, sometimes in combination with HSI model as well. Despite this, an alternative method of making use of the color-based fire detection rules, in this work, is designed in the Lab color model to determine the regions of fire candidate. This is due to the fact that, according to the findings and experiences of authors, the fires in Lab model tend to be more visible than that in other two models (this can also be seen from Figs. 2 and 3).

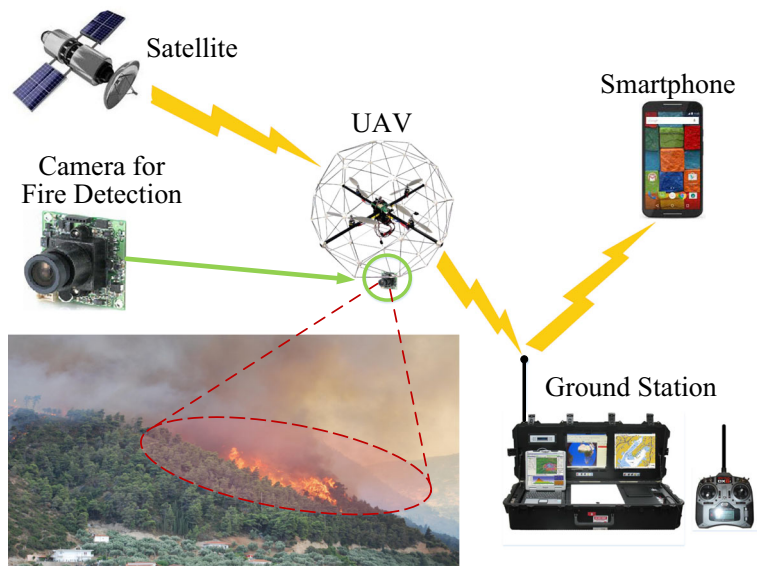

Fig. 1 General concept of the UAVs-based forest fire detection system

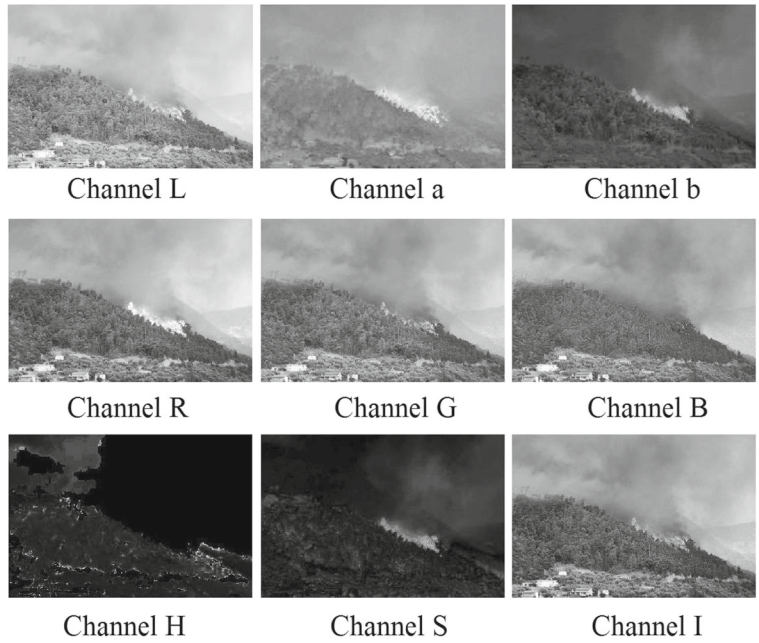

Fig. 2 Forest fires display in different color channels

As shown in Fig. 4, the Lab color model is composed of three channels: the luminance "L", the chrominance "a", and the chrominance "b". Luminance channel "L" denotes the luminance ranges from the darkest black to the brightest white. Color channel "a" indicates that the color varies from red to green, with red at positive "a" value and green at negative "a" value. Color channel "b" represents the color changes from yellow to blue, with yellow at positive "b" value and blue at negative "b" value. The scaling of "a" and "b" values are normally constrained in [−128, 127].

2.3 Horn and Schunck Optical Flow

Optical flow [35] is considered as the two dimensional distribution of apparent motion velocities of brightness patterns in an image plane. This feature can be used to estimate local pixel's movement

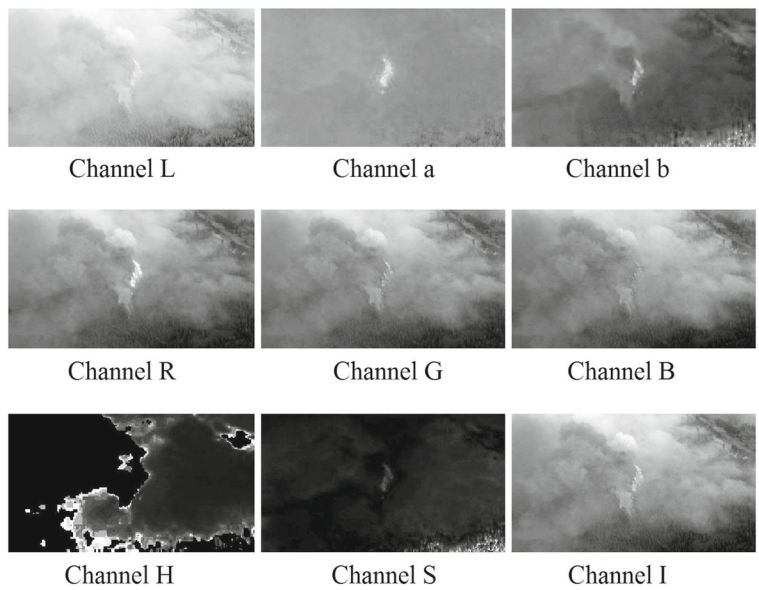

Fig. 3 Forest fires display in different color channels

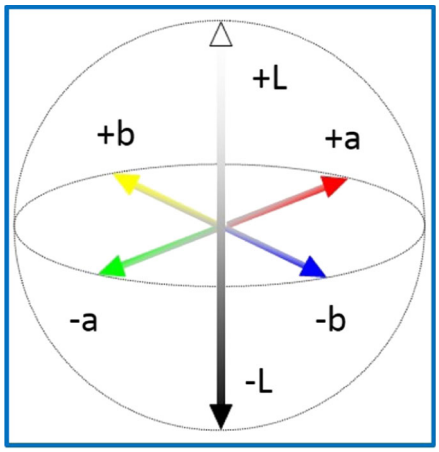

Fig. 4 Illustration of Lab color space

between two adjacent images. Each pixel in the image has one velocity vector, while these velocity vectors constitute an optical flow field. In other words, optical flow can convert image information into estimated motion fields for a more advanced analysis of features.

Horn and Schunck optical flow algorithm, which is designed based on the assumption of brightness consistency, is regarded as one of the classical optical flow calculation techniques. In mathematical representation, this assumption can be interpreted as the following constraint:

$$\frac{d}{dt}I = \frac{\partial I}{\partial x}u + \frac{\partial I}{\partial y}v + \frac{\partial I}{\partial t} = I_x u + I_y v + I_t = 0, \quad (1)$$

where $I(x, y, t)$ denotes a function of image intensity with respect to the spatial coordinates $(x, y) \in \Omega$ and time $t \in [0, T]$, while the flow vector (u, v) points to the motion direction of the pixel (x, y).

However, the single constraint (1) is insufficient for calculating the two unknowns (u, v). Additional condition is required to solve this aperture problem. In [35], Horn and Schunck suggest an effective solution hypothesizing that the optical flow is smooth over the entire image, then an estimate of the velocity (u, v) can be computed by minimizing the following constraint:

$$\int_{\Omega}\int_{0}^{T} (I_x u + I_y v + I_t)^2 + \alpha(||\nabla u||_2^2 + ||\nabla v||_2^2) dt dx dy, \quad (2)$$

where the constant α represents the smoothness term for regularization, ∇u and ∇v denote the Laplacians of u and v, respectively, which are defined as follows:

$$\nabla^2 u = \frac{\partial^2 u}{\partial^2 x} + \frac{\partial^2 u}{\partial^2 y} \quad \text{and} \quad \nabla^2 v = \frac{\partial^2 v}{\partial^2 x} + \frac{\partial^2 v}{\partial^2 y}. \quad (3)$$

Finally, (u, v) is obtainable by minimizing (2) and solving the following two iterative equations:

$$u_{x,y}^{n+1} = \bar{u}_{x,y}^{n} - \frac{I_x[I_x \bar{u}_{x,y}^{n} + I_y \bar{v}_{x,y}^{n} + I_t]}{\alpha^2 + I_x^2 + I_y^2},$$
$$v_{x,y}^{n+1} = \bar{v}_{x,y}^{n} - \frac{I_y[I_x \bar{u}_{x,y}^{n} + I_y \bar{v}_{x,y}^{n} + I_t]}{\alpha^2 + I_x^2 + I_y^2}, \quad (4)$$

where n is an iteration integer, $[u_{x,y}^{n}, v_{x,y}^{n}]$ represents the velocity estimates for the pixel at (x, y) and for $n = 0$, the initial velocity is set as zero, while $[\bar{u}_{x,y}^{n}, \bar{v}_{x,y}^{n}]$ denotes the neighborhood average of $[u_{x,y}^{n}, v_{x,y}^{n}]$.

3 Vision-Based Forest Fire Detection

The presented forest fire detection technique, in this paper, has employed both color and motion features of fire. The combination of these two features is intended to greatly enhance the reliability of forest fire detection. Color features are extracted using color-based decision making rules, while motion features are identified with optical flow which is an important technique for motion analysis in machine vision applications. The architecture of the proposed forest fire detection methodology is introduced in Fig. 5, which consists of three procedures: color detection, motion detection, and fire classification.

To be specific, Fig. 5 can likewise be introduced as follows:

1. The captured images are first converted into Lab color model, a succeeding image processing technique is employed to segment the potential fire candidates regions.
2. Based on these segmented pixels, a motion-based fire detection method is then used to make a further confirmation.
3. Finally, the further confirmed fires are to be tracked by a Blob Counter and a fire alarm and potential fire images are sent to the ground station and firefighters; otherwise, the camera keeps on capturing new images for processing.

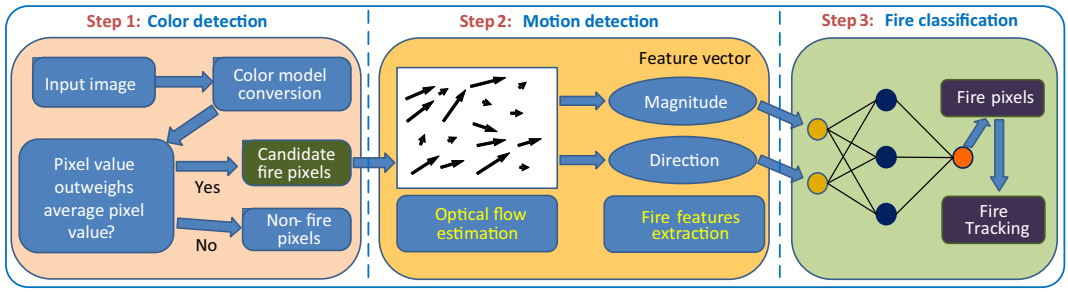

Fig. 5 Illustration of the proposed forest fire detection architecture

3.1 Color-Based Forest Fire Detection

In this research, the predominant image processing algorithms applied for automatic forest fire detection include image collection, image preprocessing (including image enhancement, color model conversion), and threshold segmentation. The organization of these algorithms can be briefly described in Fig. 6. An example of the results of the proposed color-based fire detection is also shown in Fig. 7 for providing readers a clearer picture.

3.1.1 Lab Color Model Based Fire Analysis

As most visible range cameras capture videos in the format of RGB, in order to implement the proposed concept of fire detection, there is a necessity of converting images from RGB model to Lab color model, then the values for L, a, and b can be achieved as follows:

$$\begin{aligned} L &= 116 \times (0.299R + 0.587G + 0.114B)^{1/3} - 16, \\ a &= 500 \times [1.006 \times (0.607R + 0.174G + 0.201B)^{1/3} \\ &\quad -(0.299R + 0.587G + 0.114B)^{1/3}], \\ b &= 200 \times [(0.299R + 0.587G + 0.114B)^{1/3} \\ &\quad -0.846 \times (0.066G + 1.117B)^{1/3}], \end{aligned} \tag{5}$$

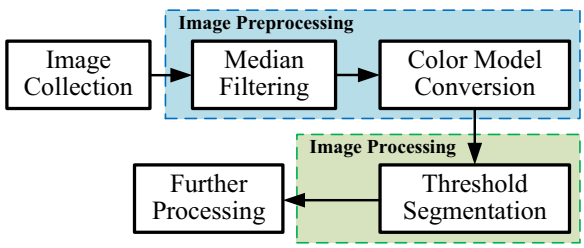

Fig. 6 Fire segmentation in Lab color model

where R, G, and B represent the values of red, green, and blue in RGB model, respectively.

In addition, fire color is typically close to red and yellow, and possesses high luminance. It is possible to assume that the values of fire pixels in each channel of Lab color model should be higher than that of other non-fire color pixels. Then, the color decision making rules in Lab color model can be formulated according to this assumption.

3.1.2 Color Based Fire Regions Identification

In each frame I, the average value $\bar{A}_I$ of fire pixels in each channel is calculated as follows:

$$\bar{A}_I = \frac{1}{N} \sum_{(x,y)\in I} P_\Phi(x, y), \tag{6}$$

where $P_\Phi(x, y)$ is the values of each pixel (at position (x, y)) for three channel components (L, a, b) in the image plane I, N denotes the number of pixels in the image.

Finally, the decision making rules (P_{FC}) for the fire-colored pixels (FC) are established as follows:

$$\begin{aligned} P_{FC} &= \begin{cases} 1, & \text{if } (P_\Phi(x, y) > \bar{A}_I), \\ 0, & \text{otherwise}, \end{cases} \\ \bar{A}_I &= \frac{1}{N} \sum_{(x,y)\in I} P_\Phi(x, y). \end{aligned} \tag{7}$$

It is worth-mentioning that the pixel is identified as fire-colored pixel if $P_\Phi(x, y)$ outweighs the threshold $\bar{A}_I$, and (P_{FC}) is set to be 1, which means that the pixel is preserved for the further analysis by motion-based fire detection approach. Otherwise, the pixel is set to be zero which indicates that the pixel is discarded without further processing.

Fig. 7 Fire segmentation in Lab color model

3.2 Motion-Based Forest Fire Detection

In general, the detection methods solely concerning objects reflecting fire color are considered as unreliable and tending to increase false alarm rates, additional features analysis of fire and more effective techniques are thereby highly demanded to improve the performance of fire detection. Normally, the fire reflects dynamic features, while the airflow produced by wind can further cause a sudden and dramatic oscillation of the fire [22]. These dynamic features make the motion detection methods being widely adopted in vision-based detection applications by extracting the moving objects, while removing the stationary non-fire regions from images. Therefore, optical flow is employed in this paper thanks to its merits in achieving motion detection with further analysis of moving regions so that non-fire moving objects can be excluded.

In particular, the camera used for capturing images is mounted on the UAV, which is moving during the entire mission period. This special property can seriously degrade the performance of fire detection, since all objects in the view are moving. In order to solve this challenging issue, this study suggests a new solution to separate the variations in the images caused by the movement of the UAV from those caused by fire.

The main concept of the proposed approach is the calculation of the discrepancies between an artificial optical flow and an optimal mass transport (OMT) optical flow [34], and extraction of the fire regions from the obtained discrepancies. The design architecture of the proposed method is illustrated in Fig. 8.

3.2.1 Optimal Mass Transport Optical Flow

Classical optical flow models are inadequate to model the appearance of fire due to their heavy dependence on the brightness constancy ($\frac{d}{dt}I = 0$). This issue is caused by two reasons:

- Due to fast pressure and heat dynamics, fast variation of intensity occurs in the burning process, therefore the assumption of intensity constancy in Eq. 1 cannot be satisfied.
- Turbulent such as non-smooth and moving fire field may be induced since smoothness regularization is counter-productive to the estimation of fire motion.

Considering the above-mentioned reasons, the OMT optical flow is expected to be a suitable choice for the fire detection. In OMT, the optical flow problem is treated as a generalized mass (which denotes image intensity I in this study) transport problem,

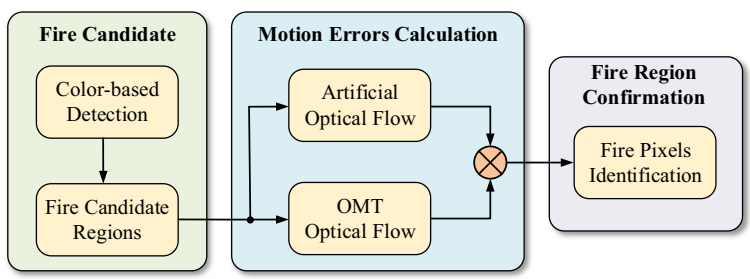

Fig. 8 Design architecture of the motion-based fire identification methodology

where a mass conservation is enforced by the data term. The conservation law can be formulated as:

$$I_t + \nabla\cdot(\mathbf{u}I) = 0, \tag{8}$$

where $\mathbf{u} = (u, v)^T$. The intensity I is replaced by mass density.

Similar to the classical optical flow, the OMT optical flow model minimizes the total energy according to:

$$\min_{\mathbf{u}} \frac{1}{2}\int_{\Omega}\int_{0}^{T} (I_t + \nabla\cdot(I\mathbf{u}))^2 + \alpha||\mathbf{u}||_2^2 I dt dx dy, \tag{9}$$

and subjects to the boundary conditions $I(x, y, 0) = I_0(x, y)$ and $I(x, y, 1) = I_1(x, y)$, where I_0 and I_1 are given gray-scale images. The transport energy $||\mathbf{u}||_2^2 I$, which is the consumption required to move mass from one location at $t = 0$ to another at $t = 1$, represents the regularization term in Eq. 9. The solution to this minimization problem can be obtained through discretizing (9):

$$\min_{\mathbf{u}} \frac{\alpha}{2}(\mathbf{u}^T\hat{I}\mathbf{u}) + \frac{1}{2}(I_t + [D_x I D_y I]\mathbf{u})^T(I_t + [D_x I D_y I]\mathbf{u}), \tag{10}$$

where $\mathbf{u}$ is a column vector containing u and v, and $\hat{I}$ is a matrix containing the average intensity values $(I_0 + I_1)/2$ on its diagonal. The derivatives are discretized by $I_t = I_1 - I_0$ and the central-difference sparse-matrix derivative operators D_x and D_y.

Equation 10 can be rewritten as:

$$\min_{\mathbf{u}} \frac{\alpha}{2}(\mathbf{u}^T\hat{I}\mathbf{u}) + \frac{1}{2}(A\mathbf{u} - b)^T(A\mathbf{u} - b), \tag{11}$$

where $A = [D_x I \; D_y I]$ and $b = -I_t$.

The solution of Eq. 11 can then be obtained as:

$$\mathbf{u} = (\alpha\hat{I} + A^T A)^{-1}(A^T b). \tag{12}$$

In addition, the generalized mass of a pixel can be represented by its similarity to a center fire color in the HSV color space ($H, S, V \in [0, 1]$). The center fire color can be properly chosen as $H_c = 0.083$, $S_c = V_c = 1$ [34], which denotes a fully color-saturated and bright orange. Then, the generalized mass can be achieved as:

$$I = f(\min\{|H_c - H|, 1 - |H_c - H|\})\cdot S\cdot V, \tag{13}$$

where f can be written into the following logistic function:

$$f(x) = 1 - (1 + \exp(-a\cdot(x - b)))^{-1}, \tag{14}$$

where $a = 100$ and $b = 0.11$.

3.2.2 OMT Optical Flow Feature Extraction

Since the main concern of this study is the pixels in movement, thus these essential pixels ($\Omega_e \subset \Omega$) can be defined as:

$$\Omega_e = \{(x, y) \in \Omega : ||\mathbf{u}(x, y)||_2 > c\cdot\max_{\Omega}||\mathbf{u}||_2\}, \tag{15}$$

where $0 \le c < 1$ is selected so that sufficient number of pixels can be retained, $\Omega \subset \Re^2$ denotes an image region.

In this work, two features $f_i : \mathbf{u} \mapsto \Re, i = 1, 2$ defining the two dimensional feature vector $F = (f_1, f_2)^T$ are chosen to conduct feature extraction. To be more specific, the magnitude feature f_1 measures mean magnitude, while the directional feature f_2 is to analyze motion directionality.

Therefore, given the image region Ω and the OMT optical flow field in this region, the magnitude and directional features are selected according to the following procedures.

1. OMT Transport Energy:

$$f_1 = \underset{\Omega_e}{Mean}\left(\frac{I}{2}||\mathbf{u}_{OMT}||_2^2\right), \tag{16}$$

   this feature is to measure the mean OMT transport energy per pixel in a subregion.
2. OMT Source Matching: For rigid motion, the flow field tends to be comprised of parallel vectors indicating rigid translation of mass. This feature is designed to quantify how well an ideal source flow template matches the computed OMT flow field, which is designed as:

$$\mathbf{u}_T(x, y) = \begin{pmatrix} u_T(x, y) \\ v_T(x, y) \end{pmatrix} = \exp\left(-\sqrt{x^2 + y^2}\right)\begin{bmatrix} x \\ y \end{bmatrix}. \tag{17}$$

Then, the best match can be obtained by:

$$f_2 = \max_{\Omega}\left|(u_T * \frac{u_{OMT}}{||\mathbf{u}_{OMT}||_2}) + (v_T * \frac{v_{OMT}}{||\mathbf{u}_{OMT}||_2})\right|, \tag{18}$$

where $*$ denotes convolution.

3.2.3 Motion Errors Calculation

After generating two optical flows using artificial optical flow for estimating the motion of camera and OMT

optical for calculating the movements of pixels in the entire image, a subsequent procedure is to compare these two obtained optical flows and compute their differences.

As shown in Fig. 9, the artificial optical flow estimates the identical moving direction of the view in the image, while the OMT optical flow identifies the motion of each pixels in the image. After that, two optical flows are incorporated together in the same image. As there is a fire presenting in this scenario, the OMT optical flow displays some apparent difference of movements among pixels. This phenomenon is caused by the intrinsic properties of fire, such as oscillation and motion irregularity with various shapes and velocities.

3.2.4 Motion Based Fire Regions Identification and Tracking

To identify the pixels in the image as fire, background, or other uninterested moving objects, the following specific fire identification procedure is required:

1. Based on the calculated moving direction of each pixel (f_2) using the OMT optical flow and the estimated moving direction of the camera coordinate frame (f_α) using the artificial optical flow, the residual between them can be obtained by $\Delta f = f_\alpha - f_2$. It is worth-mentioning that f_α is selected as the average value of directions of all pixels in the image so as to reduce the disturbance of noises and some unexpected errors.

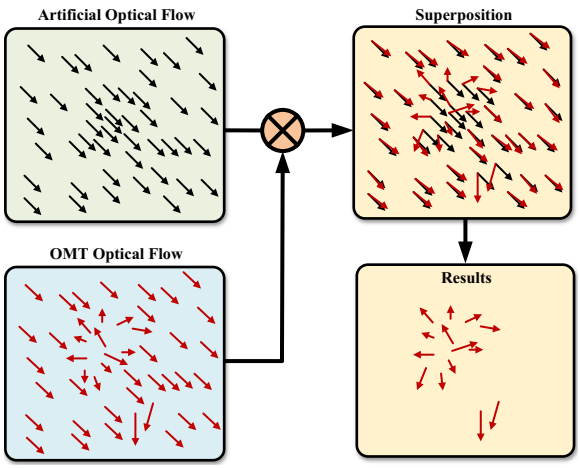

Fig. 9 Illustration of the fire pixels identification

2. This paper suggests a possible but relatively simple way of identifying fire pixels, which is to compare the angle difference of each pixel with a well selected threshold. A predefined decision making rule is then established for filtering the background and extracting the fire candidate regions. This rule is made as follows:

$$P_{FM} = \begin{cases} 1, & \text{if } \Delta f > \bar{f}, \\ 0, & \text{otherwise}, \end{cases} \tag{19}$$

where (P_{FM}) is the binarized values of pixels after fire moving (FM) pixels decision making. If Δf is over the threshold $\bar{f}$, the pixel is regarded as fire pixel and set to one, otherwise the pixel is set to zero. The threshold value can be determined according to the practical situation or by using advanced artificial intelligent methods, such as support vector machine (SVM), neural network (NN), and fuzzy logic.

In order to remove the existing small irrelative objects after the aforementioned processing and improve the ultimate fire detection performance, this study suggests to employ the morphological operations [38] to eliminate the small uninterested objects in the thresholding images.

Morphological operations, which can effectively remove small irrelative objects in the thresholding images, contain a series of operators, such as dilation, erosion, opening, and closing. This paper applies the dilation operation after erosion operation. The erosion operation E can get rid of pixels on the object boundaries, while the dilation operation D can add pixels into the images. These two operations can be defined as follows:

$$\begin{aligned} E &= I \otimes C = \{(i,j) | C_{ij} \subseteq I\} \\ D &= I \oplus C = \{(i,j) | [\hat{(C)}_{ij} \cap I] \neq \Phi\}, \end{aligned} \tag{20}$$

where symbols $\otimes$ and $\oplus$ denote the erosion operation and dilation operation, respectively. (i, j) represents the coordinates of pixel, I is image set, and C is morphological element.

Due to the simplicity and effectiveness of Blob Counter method in applications, this research work chooses it for fire tracking. Borrowing the advantages of Blob Counter capable of tracking the number and direction of blobs traversing a specific passage/entrance per unit time, the general working principle is designed as follows:

– Images are converted to binary images after the fire is ultimately identified and segmented from the background.
– The objects can then be identified based on the pixel connectivity. After that, a specific area of interest is created for each object which is labelled and assigned with a set of coordinates.
– Finally, the tracked objects are separated from the image, their number and position information are all achievable, and the fire regions are effectively tracked and located in images [39].

4 Control Design for Unmanned Aerial Vehicle

In order to search for forest fires in a specific area and obtain the aerial images using cameras, the UAV is required to be deployed for achieving these goals. Therefore, a well designed control strategy is also demanded for the operation of UAV. In this study, a combination of sliding mode control (SMC) and linear quadratic regulator (LQR) is presented for the control of UAV. The design of UAV's control architecture can be divided into two loops, the inner-loop and outer-loop. The LQR is used in the outer-loop to control the positions of UAV, while the sliding mode control, which is responsible for the attitude stabilization, is adopted in the inner-loop. Furthermore, as a kind of nonlinear controller, the use of SMC combining with the UAV's nonlinear dynamics is intended to improve the system accuracy and robustness. A brief explanation of the control system is illustrated in Fig. 10.

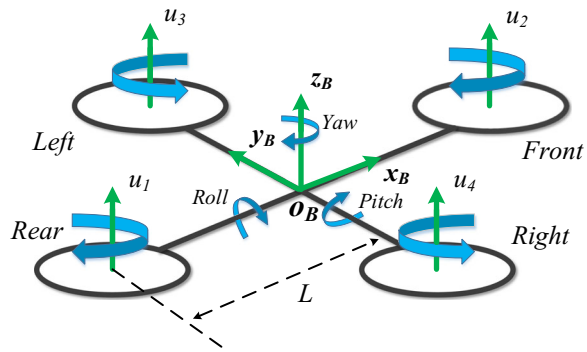

Fig. 11 Schematic diagram of a general UQH

4.1 Nonlinear Model of Unmanned Quadrotor Helicopter

Figure 11 shows a typical unmanned quadrotor helicopter (UQH), which is cooperatively operated by four direct current (DC) motor-driven propellers configured at the front, rear, left, and right corners, respectively. Thrusts u_1, u_2, u_3, and u_4 are generated by these propellers. The front and rear propellers rotate clockwise, while the right and left propellers spin counter-clockwise. The totally created thrusts always direct upward along the z_B-direction. Hence, the vertical translation is performed by straightforwardly distributing identical amount of control signal to each motor, while the horizontal translation is obtained by assigning a distinctive amount of control signals to the opposite motors, so that the UQH can roll/pitch towards the slowest motor, the lateral/forward movement can then be achieved [12].

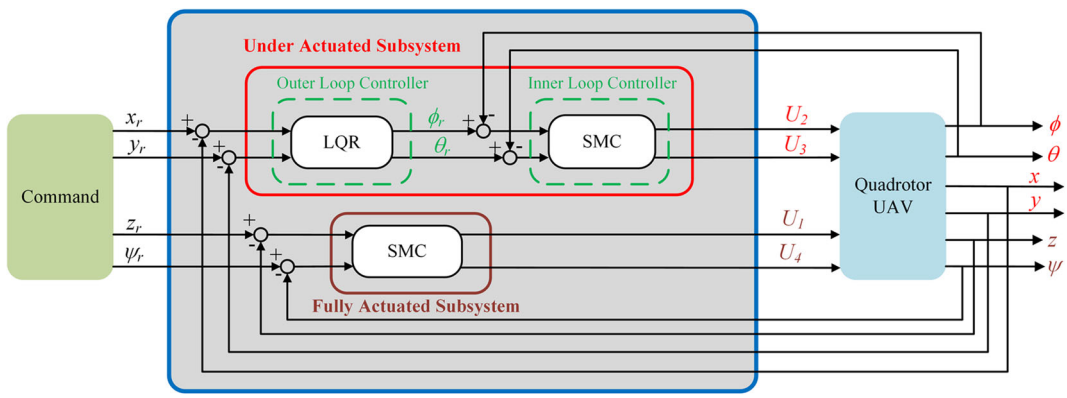

Fig. 10 Block diagram of the employed UAV control system

As described in [12], a typical UQH dynamic model with respect to the earth-fixed coordinate system can be represented as:

$$\begin{aligned}
\ddot{x} &= \frac{(sin\psi sin\phi + cos\psi sin\theta cos\phi)u_z(t) - K_1\dot{x}}{m} \\
\ddot{y} &= \frac{(sin\psi sin\theta cos\phi - cos\psi sin\phi)u_z(t) - K_2\dot{y}}{m} \\
\ddot{z} &= \frac{(cos\theta cos\phi)u_z(t) - K_3\dot{z}}{m} - g \\
\ddot{\phi} &= \frac{u_\phi(t) - K_4\dot{\phi}}{I_x} \\
\ddot{\theta} &= \frac{u_\theta(t) - K_5\dot{\theta}}{I_y} \\
\ddot{\psi} &= \frac{u_\psi(t) - K_6\dot{\psi}}{I_z}.
\end{aligned} \tag{21}$$

Furthermore, the relationship between accelerations and lift/torques is:

$$\begin{bmatrix} u_z(t) \\ u_\theta(t) \\ u_\phi(t) \\ u_\psi(t) \end{bmatrix} = \begin{bmatrix} 1 & 1 & 1 & 1 \\ L & -L & 0 & 0 \\ 0 & 0 & L & -L \\ C_m & C_m & -C_m & -C_m \end{bmatrix} \begin{bmatrix} u_1(t) \\ u_2(t) \\ u_3(t) \\ u_4(t) \end{bmatrix}. \tag{22}$$

The force and its corresponding pulse width modulation (PWM) signal owns the following relationship:

$$u_i(t) = K_m \frac{\omega_m}{s + \omega_m} u_{ci}(t). \tag{23}$$

The definitions of the above-mentioned symbols are all summarized in Table 1.

4.2 Control Schemes Design

Generally, dealing with nonlinear systems and controllers may significantly increase the computational time; meanwhile, the inherent property of SMC may likewise cause chattering effects to the system. The proposed approach, which is expected to reduce the adverse effects of the above-mentioned problems and dramatically improve system performance, combines the linear controller as LQR with SMC.

In this study, the quadrotor dynamic model [12] is divided into two subgroups due to its nonholonomic features, which can be rewritten as follows:

$$\begin{bmatrix} \ddot{z} \\ \ddot{\psi} \end{bmatrix} = \begin{bmatrix} \frac{u_z(t)}{m}\cos\theta\cos\phi - g \\ \frac{u_\psi(t)}{I_z} \end{bmatrix}, \tag{24}$$

Table 1 Nomenclature (earth-fixed coordinate system)

Symbols	Explanation
x, y, z	Coordinates of UQH at center of mass
θ	Pitch angle
ϕ	Roll angle
ψ	Yaw angle
$u_z(t)$	Total lift force
$u_\theta(t)$	The applied torque in θ direction
$u_\phi(t)$	The applied torque in ϕ direction
$u_\psi(t)$	The applied torque in ψ direction
K_n $(n = 1, 2, ..., 6)$	Drag coefficients
$u_i(t)$ $(i = 1, 2, 3, 4)$	Thrust of each rotor
L	Center distance between the gravity of UQH and each propeller
C_m	Thrust-to-moment scaling factor
g	Acceleration of gravity
m	UQH mass
I_x	Moment of inertia along x direction
I_y	Moment of inertia along y direction
I_z	Moment of inertia along z direction
ω_m	Actuator bandwidth
K_m	A positive gain
$u_{ci}(t)$ $(i = 1, 2, 3, 4)$	PWM signals distributed to each rotor

and an under-actuated subsystem is defined as:

$$\begin{bmatrix} \ddot{x} \\ \ddot{y} \end{bmatrix} = \frac{u_z(t)}{m} \begin{bmatrix} \cos\psi & \sin\psi \\ \sin\psi & -\cos\psi \end{bmatrix} \begin{bmatrix} \sin\theta\cos\phi \\ \sin\phi \end{bmatrix},$$
$$\begin{bmatrix} \ddot{\phi} \\ \ddot{\theta} \end{bmatrix} = \begin{bmatrix} \frac{u_\phi(t)}{I_x} \\ \frac{u_\theta(t)}{I_y} \end{bmatrix}. \tag{25}$$

The fully actuated subsystem controller objective is to minimize the altitude and yaw angle errors e_z and e_ψ respectively. The SMC adopted in this work is intended to achieve this goal. The following conditions should be satisfied:

$$\begin{aligned}
\lim_{t\to\infty} \|e_z\| &= \|z_r - z\| = 0 \\
\lim_{t\to\infty} \|e_\psi\| &= \|\psi_r - \psi\| = 0,
\end{aligned} \tag{26}$$

where z_r and ψ_r are the desired altitude and yaw angle respectively. The control laws for the altitude and yaw angle can be derived using classical SMC theory [40]:

$$\hat{u}_z(t) = \left(\frac{m}{\cos\theta\cos\phi}\right)(g + \ddot{z}_r - \lambda_z\dot{e}_z) \tag{27}$$

$$\hat{u}_\theta(t) = I_z(\ddot{\psi} - \lambda_\psi\dot{e}_\psi), \tag{28}$$

where λ_z and λ_ψ are control gains with $\lambda_z > 0$ and $\lambda_\psi > 0$. A discontinuous term is added across the surface $s = 0$ to satisfy the sliding condition such that:

$$U = \hat{U} - k\,\mathrm{sgn}(s), \tag{29}$$

where

$$\mathrm{sgn}(s) = \begin{cases} +1 & \text{if } s > 0 \\ -1 & \text{if } s < 0. \end{cases} \tag{30}$$

In order to facilitate the control design procedure, a further simplified model is normally preferred other than the nonlinear model (21). Before proceeding to the model simplification, the following assumptions are required:

Assumption 1 *It is assumed that the UQH is in hovering condition during the entire flight period* [12], *which implies* $u_z(t) \approx mg$. *The deflections of pitch and roll motions are so small that* $sin\phi \approx \phi$ *and* $sin\theta \approx \theta$. *There is no yaw motion such that* $\psi = 0$. *UQH moves in low velocity so that the effects from the drag coefficients are insignificant.*

Based on Assumption 1, nonlinear model (21) can be reduced into:

$$\begin{aligned} \ddot{x} &= \theta g \\ \ddot{y} &= -\phi g \\ \ddot{z} &= u_z(t)/m - g \\ I_x\ddot{\theta} &= u_\theta(t) \\ I_y\ddot{\phi} &= u_\phi(t) \\ I_z\ddot{\psi} &= u_\psi(t). \end{aligned} \tag{31}$$

As the time constant of DC motor is much smaller than that of UQH [37], Eq. 23 can be further simplified to:

$$K_m \frac{\omega_m}{s + \omega_m} \approx K_m. \tag{32}$$

Therefore, combining with Eqs. 32 and 22 can be rewritten as follows:

$$\begin{bmatrix} u_z(t) \\ u_\theta(t) \\ u_\phi(t) \\ u_\psi(t) \end{bmatrix} = \begin{bmatrix} K_m & K_m & K_m & K_m \\ K_m L & -K_m L & 0 & 0 \\ 0 & 0 & K_m L & -K_m L \\ K_m C_m & K_m C_m & -K_m C_m & -K_m C_m \end{bmatrix} U_c, \tag{33}$$

where $U_c = [u_{c1}(t), u_{c2}(t), u_{c3}(t), u_{c4}(t)]^T$.

The objective of the outer-loop controller is to obtain the desired position in x and y axes. This is achieved by applying a LQR to the following quadrotor linear dynamic model based on Assumption 1:

$$\begin{aligned} \ddot{y} &= -\phi g \\ \ddot{x} &= \theta g. \end{aligned} \tag{34}$$

Written into state-space representation, the combination of Eqs. 33 and 34 becomes:

$$\dot{x}(t) = Ax(t) + Bu(t), \tag{35}$$

where $x(t) = [\dot{x}, \dot{y}]^T \in \Re^n$ is the state vector, $u(t) = [\theta, \phi]^T \in \Re^m$ denotes the control input, and $A = \begin{bmatrix} 0 & 0 \\ 0 & 0 \end{bmatrix}$ and $B = \begin{bmatrix} g \\ -g \end{bmatrix}$.

This controller aims to find the feedback control gain K of the optimal control input u such that $u(t) = -Kx(t)$, in order to minimize the following quadratic cost function:

$$J = \int_0^\infty (x^T Q x + u^T R u) dt, \tag{36}$$

where Q and R are the weighting matrices with $Q > 0$ and $R > 0$, respectively. K can be obtained by solving the Ricatti equation.

In addition, SMC is used for the inner-loop control design which is applied to generate the control inputs $u_\phi(t)$ and $u_\theta(t)$ to satisfy accurate quadrotor attitude stabilization. This controller's objective is to converge the actual values of Euler angles ϕ and θ to their desired values ϕ_r and θ_r, which are obtained from the outer-loop controller. The corresponding control laws can be derived as:

$$\hat{u}_\phi(t) = I_x(\ddot{\phi} - \lambda_\phi \dot{e}_\phi) \tag{37}$$

$$\hat{u}_\theta(t) = I_y(\ddot{\theta} - \lambda_\theta \dot{e}_\theta), \tag{38}$$

where λ_θ and λ_ϕ are control gains with $\lambda_\theta > 0$ and $\lambda_\phi > 0$. e_ϕ and e_θ are the errors in roll and pitch angles, $e_\phi = \phi_r - \phi$ and $e_\theta = \theta_r - \theta$. ϕ_r and θ_r are the desired roll and pitch angles respectively. To satisfy the sliding conditions, Eq. 29 should be applied.

5 Experimental Results

This work chooses a forest fire video from website and a real-time fire video captured from a UAV in the lab for verifying the effectiveness of the proposed forest fire detection algorithm. Both experiments are

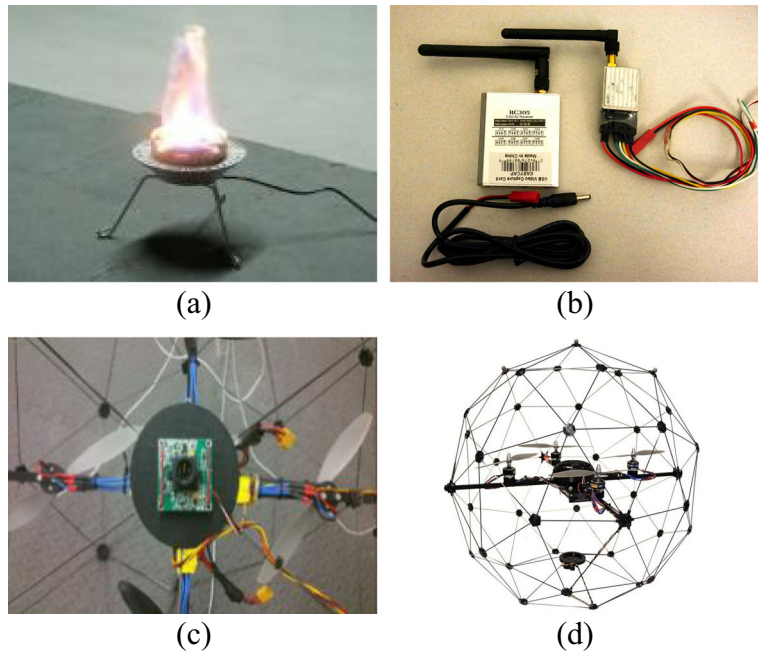

Fig. 12 Experimental equipments: **a** fire simulator, **b** FPV wireless system, **c** installed camera, and **d** Qball-X4 UAV

conducted in Matlab/Simulink environment. A desktop with Windows 7 operating system, Intel core $i7$ processor and $8GB$ memory is employed for image processing and data display.

5.1 Scenarios Description

In order to achieve a clear and effective evaluation of the proposed algorithm, the following scenarios are selected:

1. *Scenario 1*: A real aerial video of forest fire borrowed from the website (https://www.youtube.com/watch?v=up3kuTwBpsw) is used for the validation of the proposed fire detection approach. The resolution of the video is 640 × 360.
2. *Scenario 2*: In order to demonstrate the efficacy of the developed UAV-based forest fire detection methodology in practical applications, a UAV-based forest fire detection system is employed for the indoor experimental test.

   As shown in Fig. 12, several components are included in this system:

   – As no GPS signal is available indoor, a network of cameras system works as the global positioning system (GPS) to offer the UAV with 3-dimensional (3D) position information.
   – A UQH is deployed for carrying payloads (visual cameras) for fire searching and detection.
   – A visual camera along with a wireless communication system (includes a 5.8 GHz 200 mW transmitter and a 5.8 GHz AV receiver) are installed at the bottom of the UQH to capture and transfer real-time images to the ground station. Table 2 lists the specification of the adopted camera.
   – A fire simulator is used for creating the simulative fire which is deemed as the target fire.
   – A ground station is set up for planning and distributing tasks to UQH to execute, as well

Table 2 Specification of adopted camera

Parameter	Description
Image device	1/3-inch Sony color CCD
Resolution	752 × 582
Auto backlight compensation	On/off switchable
Minimum illumination	0.1Lux/F1.2
S/N ratio	Greater than 48 dB
White balance	Auto tracking
Power supply	12 V/150 mA
Lens	3.6–6 mm

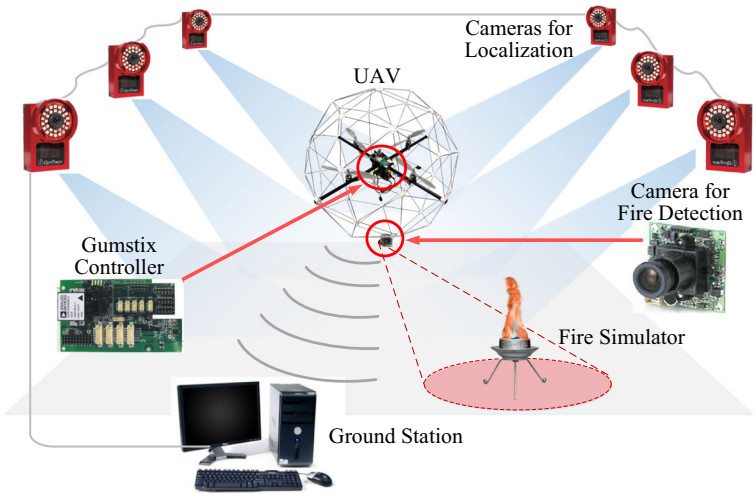

Fig. 13 Layout of the used UAV-based forest fire search and detection system

as displaying and processing real-time images obtained from onboard camera.

Furthermore, Fig. 13 provides an overview of the adopted experimental platform and environment. In this experimental validation, a single UAV is deployed to patrol a 4 m × 4 m square field, searching for fire spots. As displayed in Fig. 14, this UAV first starts its task from the corner of the field; following this, it patrols the assigned surveillance region along a predefined trajectory (each trajectory is 1 m apart from its neighbors); a sequence of hovering actions around the fire (each action lasts 5 s) is to be conducted once a potential fire event is detected, so as to make a further confirmation; the data collected by the UAV is to be sent to the ground station for processing. If the fire is confirmed, a fire alarm is to be triggered, otherwise the fire search mission resumes.

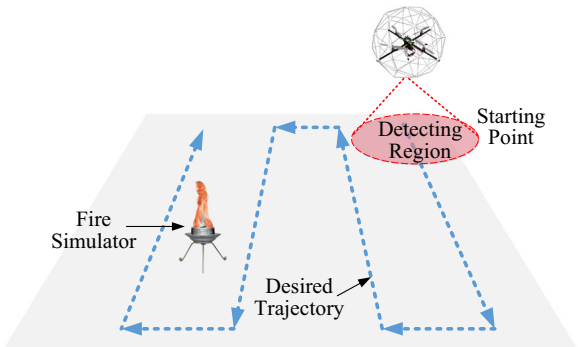

Fig. 14 General illustration of the conducted fire search and detection experiment

5.2 Results of Scenario 1

Figure 15 shows the results of the proposed fire detection algorithm which is applied to a video captured from a real forest fire. Figure 15a, e and i show the original images; color segmented results are listed in Fig. 15b, f and j); optical flow estimation and morphological operation results are displayed in Fig. 15c, g and k; while the final results of fire tracking using the Blob Counter method are displayed in Fig. 15d, h and l, respectively.

From Fig. 15b, f and j, it shows that most non-fire regions are eliminated including trees and smoke, while the remaining pixels that have passed the color-based decision making rule are considered as fire candidate regions for further analysis by motion-based detection method using optical flow approaches. Figure 15c, g and k show that, after further processing the thresholding results adopting optical flow estimation and morphological operations, the moving/static fire colored analogues such as smoke, houses, and paths in the forest can be removed using the moving regions detection rule. Finally, fires are successfully tracked by red rectangles through Blob Counter; these results can be seen in Fig. 15d, h and l.

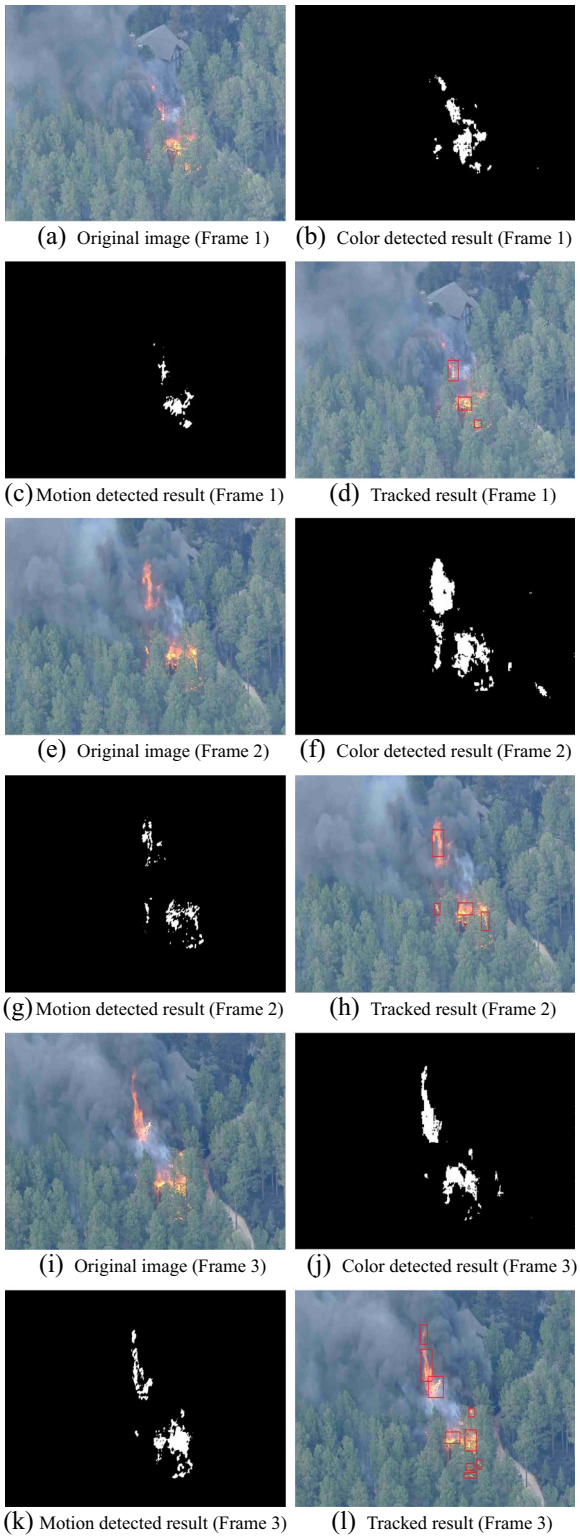

(a) Original image (Frame 1) (b) Color detected result (Frame 1)
(c) Motion detected result (Frame 1) (d) Tracked result (Frame 1)
(e) Original image (Frame 2) (f) Color detected result (Frame 2)
(g) Motion detected result (Frame 2) (h) Tracked result (Frame 2)
(i) Original image (Frame 3) (j) Color detected result (Frame 3)
(k) Motion detected result (Frame 3) (l) Tracked result (Frame 3)

Fig. 15 Experimental results of sample frames

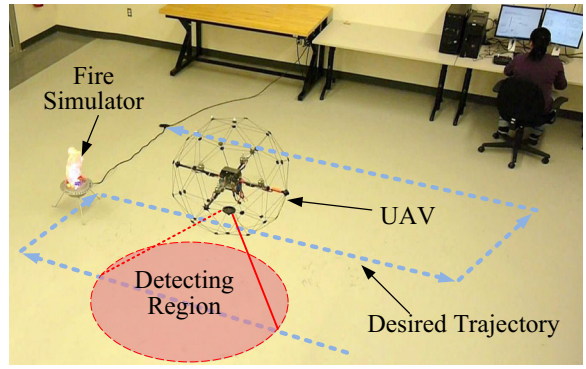

Fig. 16 Experimental scenario description in practice

5.3 Results of Scenario 2

Figure 16 provides a view of the experiment conducted in indoor environment. The real trajectory tracking performance of the deployed UAV in 3D is shown in Fig. 17. The planned trajectory is finally tracked with satisfactory performance by using the proposed control method. In order to introduce the fire search procedure in a clearer fashion, Figs. 18 and 19 are also employed. In particular, Fig. 18 indicates that the UAV hovers at three positions during the entire mission at 62th, 68th, and 74th second, respectively; and each hovering action lasts 6 seconds. Actually, these three hovering actions are intentional, which exactly explain the potential fire detection and further confirmation by deploying UAV to hover at different positions to observe the fire from different angles of views.

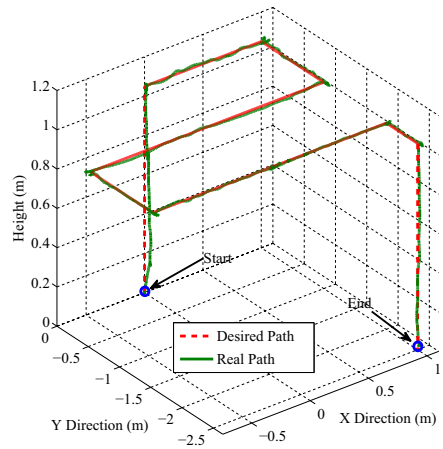

Fig. 17 Trajectory tracking performance of the UAV displayed in 3D

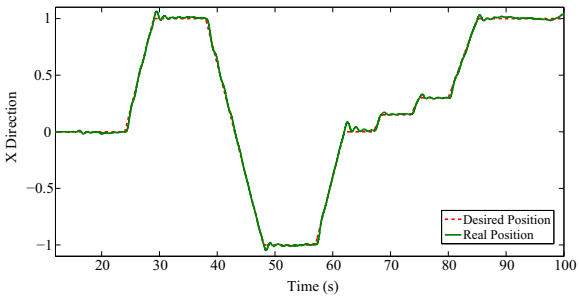

Fig. 18 Trajectory tracking performance of the UAV along X coordinate

Figure 20 shows images captured from UAV and fire detection results of the proposed algorithm. Three frames captured by the UAV from three different positions along with their corresponding image processing results are shown in Fig. 20. Similar to the layout in Fig. 15, the original images are listed in Fig. 20a, e and i; Fig. 20b, f and j show the results of color segmentation; Fig. 20c, g and k display the optical flow estimation and morphological operation results; final results of fire tracking are shown in Fig. 20d, h and l.

From Fig. 20b, f and j, it can be seen that the fire-colored regions have been successfully detected and extracted, whereas some non-fire regions with analogical color of fire, such as the lights and metal parts of the fire simulator which reflect the fire color are extracted as well. The motion-based decision making rules for finding the actual fire regions are thereby demanded to improve the performance of fire detection. The optical flow features in this work are applied for further investigating the wrongly extracted areas. Comparing with Fig. 20b, f and j, it clearly shows that non-fire regions are effectively removed in Fig. 20c, g and k.

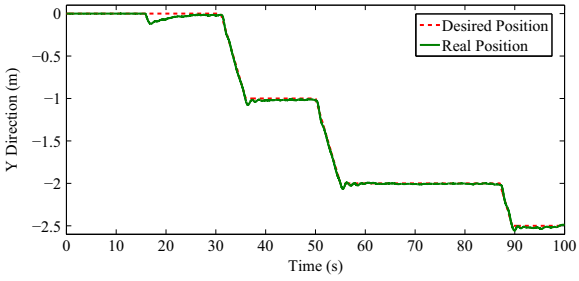

Fig. 19 Trajectory tracking performance of the UAV along Y coordinate

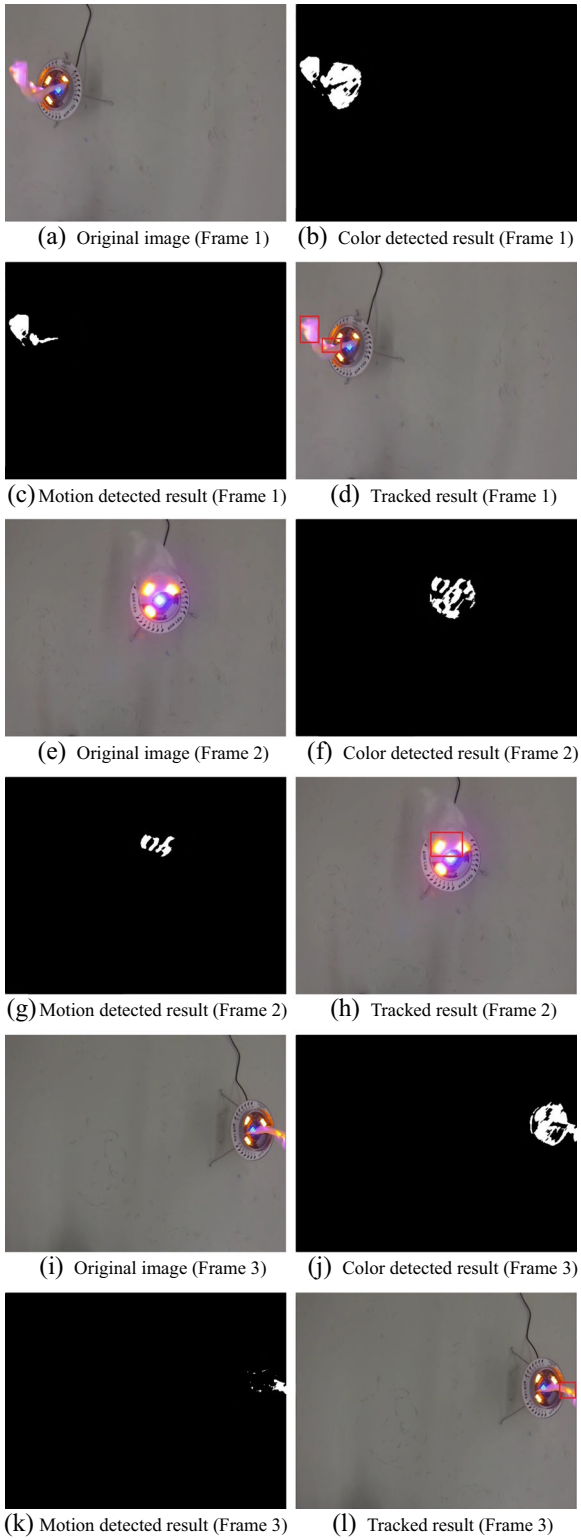

Fig. 20 Experimental results

6 Conclusions and Future Works

In this paper, a vision-based forest fire detection approach using color and motion based analysis is proposed for the application of UAV-based firefighting. The proposed method utilizes both chroma and motion characteristics of fire in the decision making rules to improve the reliability and accuracy of fire detection results. A color-based fire detection method with light computation requirement intended to effectively identify the suspicious fire regions with high accuracy is first devised. Despite the movement of all objects and background in images due to the motion of UAV, the proposed motion-based fire detection approach can further distinguish and track fires effectively from background as well as analogues such as non-fire moving objects and disturbances owning the similar color as fire. Experimental demonstrations are carried out in two scenarios, one is a real forest fire video collected from an aircraft and the other is a real-time video gathered by a UAV in an indoor environment. Experimental results have verified that the proposed forest fire detection method is capable of achieving good performance with greatly enhanced reliability and accuracy in forest fire detection applications.

Following the work presented in this paper, several potential directions can be extended. Powerful fire classification techniques such as neural network and support vector machine can be adopted and well trained to further improve the performance of forest fire detection and decrease the false fire alarm rate. In addition to that, a fire localization strategy can be developed to transform the fire image coordinates to the real position in the world coordinates.

Acknowledgments The authors would like to express their sincere gratitude to the Editors and the anonymous reviewers whose insightful comments have helped to improve the quality of this paper significantly. The authors also would like to acknowledge the financial supports from Natural Sciences and Engineering Research Council of Canada (NSERC), NSFC under Grant 61573282 and SPNSF under Grant 2015JZ020 for the work reported in this paper.

References

1. Yuan, C., Zhang, Y.M., Liu, Z.X.: A survey on technologies for automatic forest fire monitoring, detection and fighting using UAVs and remote sensing techniques. Can. J. Forest Res. **45**(7), 783–792 (2015)
2. Kolarić, D., Skala, K., Dubravić, A.: Integrated system for forest fire early detection and management. Period. Biol. **110**(2), 205–211 (2008)
3. Martinez-de Dios, J.R., Arrue, B.C., Ollero, A., Merino, L., Gómez-Rodríguez, F.: Computer vision techniques for forest fire perception. Image Vision Comput. **26**(4), 550–562 (2008)
4. Gonzalez, J.R., Palahi, M., Trasobares, A., Pukkala, T.: A fire probability model for forest stands in Catalonia (North-East Spain). Ann. For. Sci. **63**(2), 169–176 (2006)
5. Lin, H., Liu, Z., Zhao, T., Zhang, Y.: Early warning system of forest fire detection based on video technology. In: International Symposium on Linear Drives for Industry Applications, pp. 751–758 (2014)
6. Everaerts, J.: The use of unmanned aerial vehicles (UAVs) for remote sensing and mapping. Int. Arch. Photogramm. **37**, 1187–1192 (2008)
7. Berni, J.A., Zarco-Tejada, P.J., Suárez, L., Fereres, E.: Thermal and narrowband multispectral remote sensing for vegetation monitoring from an unmanned aerial vehicle. IEEE Trans. Geosci. Remote Sens. **47**(3), 722–738 (2009)
8. Yuan, C., Liu, Z.X., Zhang, Y.M.: UAVS-based forest fire detection and tracking using image processing techniques. In: International Conference on Unmanned Aircraft Systems, pp. 639–643 (2015)
9. Yuan, C., Liu, Z.X., Zhang, Y.M.: Vision-based forest fire detection in aerial images for firefighting using UAVs. In: International Conference on Unmanned Aircraft Systems, pp. 1200–1205 (2016)
10. Sharifi, F., Zhang, Y.M., Aghdam, A.G.: A distributed deployment strategy for multi-agent systems subject to health degradation and communication delays. J. Intell. Rob. Syst. **73**(1–4), 623–633 (2014)
11. Merino, L., Caballero, F., Martínez-de-Dios, J.R., Maza, I., Ollero, A.: An unmanned aircraft system for automatic forest fire monitoring and measurement. J. Intell. Robot. Syst. **65**(1-4), 533–548 (2012)
12. Liu, Z.X., Yuan, C., Zhang, Y.M., Luo, J.: A learning-based fault tolerant tracking control of an unmanned quadrotor helicopter. J. Intell. Robot. Syst., 1–18 (2015)
13. Liu, Z.X., Yu, X., Yuan, C., Zhang, Y.M.: Leader-follower formation control of unmanned aerial vehicles with fault tolerant and collision avoidance capabilities. In: International Conference on Unmanned Aircraft Systems, pp. 1025–1030 (2015)
14. Ollero, A., Arrue, B.C., Martínez-de-Dios, J.R., Murillo, J.J.: Techniques for reducing false alarms in infrared forest-fire automatic detection systems. Control Eng. Practice. **7**(1), 123–131 (1999)
15. Ferruz, J., Ollero, A.: Real-time feature matching in image sequences for nonstructured environments: applications to vehicle guidance. J. Intell. Robot. Syst. **28**(1–2), 85–123 (2000)
16. Merino, L., Caballero, F., Martínez-de-Dios, J.R., Ferruz, J., Ollero, A.: A cooperative perception system for multiple UAVs: Application to automatic detection of forest fires. J. Field Robot. **23**(3-4), 165–184 (2006)
17. Maza, I., Caballero, F., Capitán, J., Martínez-de-Dios, J.R., Ollero, A.: Experimental results in multi-UAV coordination for disaster management and civil security applications. J. Intell. Robot. Syst. **61**(1-4), 563–585 (2010)

18. Ambrosia, V.G., Wegener, S., Zajkowski, T., Sullivan, D.V., Buechel, S., Enomoto, F., Lobitz, B., Johan, S., Brass, J., Hinkley, E.: The Ikhana unmanned airborne system (UAS) western states fire imaging missions: from concept to reality (2006–2010). Geocarto Int. **26**(2), 85–101 (2011)
19. Martínez-de-Dios, J.R., Merino, L., Caballero, F., Ollero, A.: Automatic forest-fire measuring using ground stations and unmanned aerial systems. Sensors **11**(6), 6328–6353 (2011)
20. Bradley, J.M., Taylor, C.N.: Georeferenced mosaics for tracking fires using unmanned miniature air vehicles. J. Aerosp. Comput. Inf. Commun. **8**(10), 295–309 (2011)
21. Celik, T., Ozkaramanl, H., Demirel, H.: Fire pixel classification using fuzzy logic and statistical color model. In: IEEE International Conference on Acoustic Speech Signal Processing, vol. 1, pp. 1205–1208 (2007)
22. Chen, T., Wu, P., Chiou, Y.: An early fire-detection method based on image processing. In: IEEE International Conference on Image Processing, pp. 1707–1710 (2004)
23. Toreyin, B.U., Dedeoglu, Y., Cetin, A.E.: Flame detection in video using hidden Markov models. In: IEEE International Conference on Image Processing, vol. 2, pp. 1230–1233 (2005)
24. Celik, T., Demirel, H., Ozkaramanli, H., Uyguroglu, M.: Fire detection using statistical color model in video sequences. J. Visual Commun. Image Represent. **18**(2), 176–185 (2007)
25. Celik, T., Demirel, H.: Fire detection in video sequences using a generic color model. Fire Saf. J. **44**(2), 147–158 (2009)
26. Gunay, O., Tasdemir, K., Toreyin, B.U., Cetin, A.E.: Video based wildfire detection at night. Fire Saf. J. **44**(6), 860–868 (2009)
27. Gunay, O., Toreyin, B.U., Kose, K., Cetin, A.E.: Entropy-functional-based online adaptive decision fusion framework with application to wildfire detection in video. IEEE Trans. Image Process. **21**(5), 2853–2865 (2012)
28. Phillips, W., Shah, M., Lobo, N.V.: Flame recognition in video. In: IEEE Workshop on Applications of Computer Vision, pp. 224–229 (2000)
29. Ko, B.C., Cheong, K.H., Nam, J.Y.: Fire detection based on vision sensor and support vector machines. Fire Saf. J. **44**(3), 322–329 (2009)
30. Rodríguez-Canosa, G.R., Thomas, S., del Cerro, J., Barrientos, A., MacDonald, B.: A real-time method to detect and track moving objects (DATMO) from unmanned aerial vehicles (UAVs) using a single camera. Remote Sens. **4**(4), 1090–1111 (2012)
31. Miller, A., Babenko, P., Hu, M., Shah, M.: Person Tracking in UAV Video. Lecture Notes in Computer Science. Springer, Berlin/Heidelberg (2008)
32. Huang, C.H., Wu, Y.T., Kao, J.H., Shih, M.Y., Chou, C.C.: A hybrid moving object detection method for aerial images. In: Pacific-Rim Conference on Multimedia, pp. 357–368 (2010)
33. Suganuma, N., Kubo, T.: Fast dynamic object extraction using stereovision based on occupancy grid maps and optical flow. In: IEEE/ASME International Conference on Advanced Intelligent Mechatronics (AIM), pp. 978–983 (2011)
34. Mueller, M., Karasev, P., Kolesov, I., Tannenbaum, A.: Optical flow estimation for flame detection in videos. IEEE Trans. Image Process. **22**(7), 2786–2797 (2013)
35. Horn, B.K., Schunck, B.G.: Determining optical flow. Artif. Intell. **17**(1-3), 185–203 (1981)
36. Cetin, A.E., Dimitropoulos, K., Gouverneur, B., Grammalidisb, N., Gunaya, O., Habiboglua, Y.H., Töreyind, B.U., Verstockte, S.: Video fire detection–review. Digital Signal Process. **23**(6), 827–1843 (2013)
37. Stevens, B.L., Lewis, F.L.: Aircraft Control and Simulation. Wiley (2003)
38. Katić, D., Vukobratović, M.: Survey of intelligent control techniques for humanoid robots. J. Intell. Robot. Syst. **37**(2), 117–141 (2003)
39. Amit, Y.: 2D Object Detection and Recognition: Models, Algorithms, and Networks. MIT Press, Chicago: Cambridge, Mass (2002)
40. Utkin, V.I.: Sliding Modes in Control and Optimization. Springer Science & Business Media (2013)

Chi Yuan is currently a Ph.D. candidate in mechanical engineering with the Department of Mechanical and Industrial Engineering at Concordia University, Montreal, QC, Canada. Her research interests include unmanned aerial/ground vehicles-based forest fire monitoring, detection and fighting, visual and infrared image processing, data fusion, intelligent decision making, and vision based robotic navigation.

Zhixiang Liu is currently doing post-doctoral research in Loria at University of Lorraine, Nancy, France. He did his Ph.D. research in the Department of Mechanical and Industrial Engineering at Concordia University, Montreal, QC, Canada. His research interests include fault detection, diagnosis and tolerant control of safety-critical systems, collision avoidance, robotic systems design, as well as guidance, navigation, and control of unmanned aerial/ground/surface vehicles.

Youmin Zhang received the B.S., M.S., and Ph.D. degrees from Northwestern Polytechnical University, Xi'an, China, in 1983, 1986, and 1995, respectively. He is currently a Professor with the Department of Mechanical and Industrial Engineering and the Concordia Institute of Aerospace Design and Innovation, Faculty of Engineering and Computer Science, Concordia University, Montreal, Quebec, Canada. His current research interests include condition monitoring, health management, fault diagnosis, and fault-tolerant (flight) control systems, cooperative guidance, navigation, and control (GNC) and remote sensing of single and multiple unmanned aerial/space/ground/surface vehicles and their applications to forest fires, powerlines and pipelines, search and rescue monitoring, detection and services, dynamic systems modeling, estimation, identification, advanced control techniques and advanced signal processing techniques for diagnosis, prognosis, and health management of safety-critical systems, renewable energy systems and smart grids, and manufacturing processes. He has authored four books, over 400 journal and conference papers, and book chapters. He is a Senior Member of the American Institute of Aeronautics and Astronautics (AIAA) and the Institute of Electrical and Electronics Engineers (IEEE), and a member of the Technical Committee (TC) for several scientific societies, including the International Federation of Automatic Control TC on Fault Detection, Supervision and Safety for Technical Processes, the AIAA Infotech@Aerospace Program Committee on Unmanned Systems, the IEEE Robotics and Automation Society TC on Aerial Robotics and Unmanned Aerial Vehicles, the ASME/IEEE TC on Mechatronics and Embedded Systems and Applications, and the International Conference on Unmanned Aircraft Systems (ICUAS) Association Executive Committee. He has been invited to deliver plenary talks at international conferences/workshops and research seminars worldwide for over 80 times. He is an Editor-in-Chief of the Journal of Instrumentation, Automation and Systems, an Editor-at-Large of the Journal of Intelligent & Robotic Systems, and an Editorial Board Member/Associate Editor of several other international journals (including three newly launched journals on Unmanned Systems). He has served as General Chair, Program Chair, and IPC Member of many international conferences, including the General Chair of the 10th International Conference on Intelligent Unmanned Systems (ICIUS) in 2014, Montreal, Canada, the Program Chair of the International Conference on Unmanned Aircraft Systems (ICUAS) in 2014, Orlando, FL, USA, one of General Chairs of the ICUAS in 2015, Denver, USA, a Co-General Chair of the ICIUS 2016 to be held at Xian, China, and Program Chair of the ICUAS 2017 to be held at Miami, USA. More detailed information can be found at http://users.encs.concordia.ca/~ymzhang/index.html.